

Fatigue Behavior of LB-PBF Ti-6Al-4V Parts Under Mean Stress and Variable Amplitude Loading Conditions

Patricio Carrion, Nima Shamsaei*

Department of Mechanical Engineering, Auburn University, Auburn, AL 36849, USA

*National Center for Additive Manufacturing Excellence (NCAME),
Auburn University, Auburn, AL 36849, USA*

*Corresponding author: shamsaei@auburn.edu

Abstract

Additively manufactured components are intended for use in load bearing applications, which are often accompanied by fluctuating external loadings. Therefore, understanding the fatigue behavior of AM materials under variable amplitude loadings is necessary for ensuring reliable in-service component performance. This research focuses on the fatigue behavior of Ti-6Al-4V, fabricated via laser beam powder bed fusion process, under mean stress and variable amplitude loadings. Mean stress effects are investigated under strain-controlled constant amplitude loading under fully-reversed, $R_e = -1$, and tension-release, $R_e = 0$, strain ratios. The generated data is used to compare two mean stress models including Morrow and Smith-Watson-Topper. Variable amplitude loading conditions include fully reversed high-low and low-high loading to investigate load sequence and history effects. Finally, cumulative fatigue damage and life predictions are made using the linear damage accumulation model (i.e., Miner's rule).

Keywords: Additive manufacturing, Mean stress, Variable amplitude, Miner's Rule, Titanium.

Introduction

In recent years, additive manufacturing (AM) technology has come to the spotlight as a promising alternative to conventional subtractive manufacturing methods. AM allows industries to fabricate far more complex parts directly from a CAD model by melting and joining the raw material layer-by-layer [1,2]. Laser beam powder bed fusion (LB-PBF) is among one of the most commonly used AM methods, which involves spreading a thin layer of metallic powder above the built platform and melting the powder to create a solid layer of the part [1,3,4]. Although innovative, parts fabricated via LB-PBF or other AM methods, are negatively affected by inherent internal and surface defects (e.g., porosity and as-built surface roughness). These types of defects have been identified as the most detrimental to fatigue performance and overall mechanical properties [2–13]. Post-processing methods, such as machining to remove the rough surfaces, and hot isostatic pressing (HIP) to close internal defects, have been proposed as feasible solutions to improve mechanical properties and performance of AM parts [2–5]. Unfortunately, post-

processing techniques are still not able to eliminate all of the defects and improve material properties to match those of the wrought counterparts. Therefore, a current major concern is whether AM parts with minimum post-processing treatment (e.g., only stress relieving) can be integrated into load-bearing applications as a viable alternative to conventionally manufactured parts.

Under realistic service conditions, AM parts will be subjected to random asymmetric fluctuating loads; therefore, the load history and its influence on the fatigue behavior with zero and non-zero mean stresses must be considered. In recent years, only a limited number of studies have attempted to characterize the fatigue behavior of AM parts under more realistic loadings [12,14–16]. The low and high cycle fatigue behavior of LB-PBF Ti-6Al-4V ELI (extra low interstitials) under different stress ratios ($R_\sigma = -3, -1$ and 0.1) was investigated in [14]. The study concluded that the low cycle fatigue behavior is appropriately represented by the Coffin-Manson (C-M) equation, and that mean stress mainly affects fatigue behavior in the high cycle regime. Moreover, [15] focused on the variable amplitude fatigue behavior of rough as-built Ti-6Al-4V manufactured via LB-PBF and electron beam powder bed fusion (EB-PBF) process. In the study, it was demonstrated that conventional cumulative damage approaches could offer acceptable fatigue life predictions for parts subjected to fully random loading. To evaluate the load history and load sequence effects, the damage accumulated in a material under cyclic loading must be quantified. Therefore, an appropriate fatigue damage parameter (e.g., cycles to failure, crack size, stress response, etc.) must be utilized for fatigue life estimation using a suitable cumulative damage rule.

The previously mentioned studies demonstrated the existence of a knowledge gap on the prospect of integrating AM parts directly from fabrication (i.e., minimum post-processing) to load-bearing applications. Therefore, as an effort to enhance the understanding of the fatigue behavior of AM parts, this research investigates as-built/annealed LB-PBF Ti-6Al-4V parts under mean stress and variable amplitude loadings. Mean stress effects are investigated using two strain ratios ($R_\epsilon = -1, 0$). Cumulative damage, load history, and load sequence effects were studied through fully reversed high-low and low-high loading. The generated constant amplitude data is used to evaluate the ability of Morrow, and Smith-Watson-Topper (SWT) mean stress correction models to predict fatigue life. Finally, the applicability of the linear damage rule (LDR) for fatigue life prediction of tests under high-low and low-high loading is evaluated.

Experimental Procedure

Specimen fabrication and material characterization

Gas atomized Ti-6Al-4V Grade 23 metal powder with a mean particle size of ~ 30 μm manufactured by LPW Technology was selected for this study. The metal powder was used and was previously recycled. A brief explanation of the recycling/reconditioning procedure can be found in [11]. Round uniform gage section fatigue specimens were manufactured vertically using an EOS M290. The manufacturer recommended performance parameters used include 280 W laser power, 1200 mm/s scan speed, 100 mm stripe width, 140 μm hatch spacing, 67° hatch rotation, and a layer thickness of 30 μm . The uniform gage section had a 3.75 mm diameter and a 15 mm

length; these dimensions were based on ASTM E606 standard [17]. Post-manufacture, the specimens were stress relieved at 704 °C in an argon atmosphere for 1 hour, then furnace cooled to room temperature. Since only stress relief was performed, the specimens are considered to be in the “annealed as-built” condition. Microstructural characteristics of LB-PBF Ti-6Al-4V were investigated by dissecting the uniform gage section of a virgin specimen into two cross-sections: one cross-section perpendicular to the build direction, and one along the build direction. After dissection, the cross-sections were polished, etched using Kroll’s reagent, and a digital microscope was used to capture microstructure images.

Test procedures

Monotonic tensile and fatigue tests were performed using an MTS 810 servohydraulic system with a 100 kN load capacity. All tests were strain-controlled using an extensometer with a 10 mm gage length. Monotonic tensile tests (2 total) were first conducted at 0.001 s⁻¹ strain rate until 0.045 mm/mm was reached, then switched to displacement control until specimen failure. The displacement rate used was 0.015 mm/s. All fatigue tests were conducted following ASTM E606 standard [17] and using a tapered sinusoidal wave signal. For constant amplitude tests, fully reversed ($R_e = -1$) and pulsating ($R_e = 0$) loading was used. Variable amplitude tests include high-low and low-high two-level block loading. Strain amplitude, ϵ_a , values used in this study ranged between 0.001 - 0.006 mm/mm. To verify fatigue results, duplicate tests were conducted for each constant amplitude loading condition (e.g., $R_e = -1$ at different ϵ_a values), while for block loading (i.e., high-low and low-high at different ϵ_a values), three tests were conducted per condition. Experiments that reached over 4E6 reversals were determined to be a runout. Furthermore, strain rate effects on the fatigue behavior were attenuated by adjusting the test frequency in order to maintain a nearly constant average strain rate for all tests.

Results and Discussion

Microstructure

Cross-sectional views of the microstructure of LB-PBF Ti-6Al-4V perpendicular to and along the build direction are presented in **Fig. 1(a)** and (b) respectively. It can be seen from the figures that the microstructure has fine acicular α' grains surrounded by prior- β grain boundaries. From **Fig. 1(a)**, it was also observed that the grain morphology is affected by the laser scan pattern and hatch distance ($\sim 140 \mu\text{m}$), thus resulting in equiaxed grains. However, epitaxial grain growth is observed in **Fig. 1(b)**, which can be attributed to the high heat flow from the printed layer towards the relatively colder substrate, resulting in columnar grains oriented parallel to the build direction. Similar results have been observed and extensively discussed in the literature for parts manufactured via LB-PBF process [5–9,11,10].

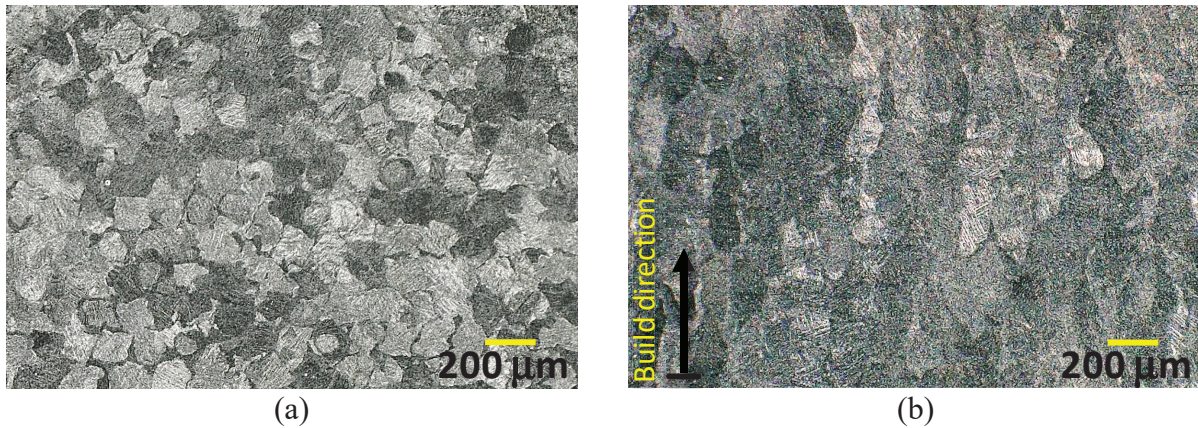


Fig. 1. Cross-sectional views of the microstructure of as-built LB-PBF Ti-6Al-4V (a) perpendicular to, and (b) along the build direction.

Monotonic tensile behavior

The monotonic stress-strain response of two LB-PBF Ti-6Al-4V specimens is presented in **Fig. 2**. As previously mentioned, the strain was recorded up to 0.0045 mm/mm, hence stress-strain curves end with arrows to indicate that the test continued in displacement control mode until specimen failure. From the stress-strain curves, it can be seen that after yielding the material exhibits almost no work hardening; as a result, the yield stress value is relatively similar to the ultimate tensile stress. This behavior could be explained by the high yield strength of the martensitic α' microstructure delaying the onset of permanent plastic deformation, but once plastic deformation occurs, the orientation of the retained prior- β grain boundaries facilitate plastic deformation as slip systems on preferred planes are activated (increasing ductility) without further increase in strength [6,18]. Moreover, due to the martensitic α' microstructure found in LB-PBF Ti-6Al-4V, the yield and ultimate tensile strength are usually higher than wrought Ti-6Al-4V, which commonly has an equiaxed microstructure [4,6,10,12,19]. Monotonic tensile results include a yield (0.2 % offset) and ultimate tensile stress of 1040 and 1080 MPa, respectively, and 17%

elongation at failure. These values are in agreement with similar studies on the mechanical behavior of as-built/annealed LB-PBF Ti-6Al-4V parts fabricated vertically [4–6,8–12].

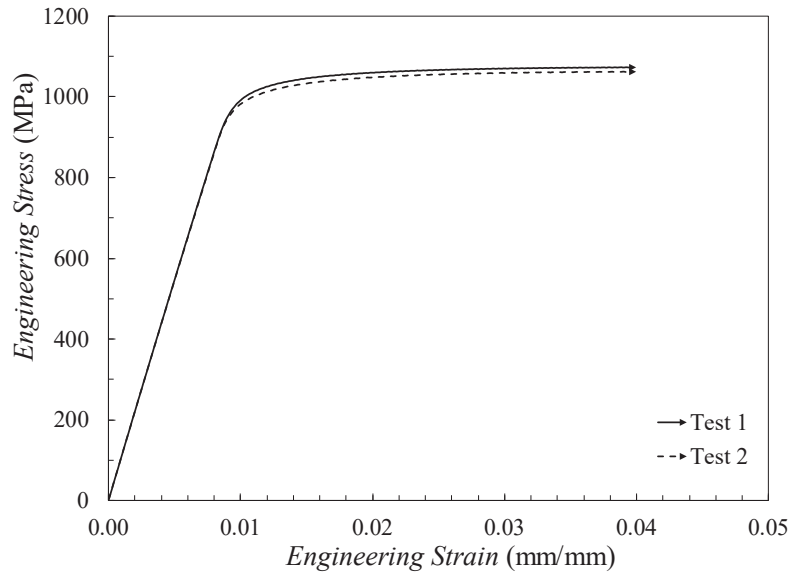


Fig. 2. Monotonic stress-strain curves of as-built LB-PBF Ti-6Al-4V generated in this study.

Fatigue behavior and mean stress models

Presented in **Fig. 3** is a semi-log plot of the strain amplitude, ε_a , versus reversals to failure, $2N_f$, for fatigue tests under $R_\varepsilon = -1$ and $R_\varepsilon = 0$ loading from this study along with fully reversed fatigue data from a powder recycling study ($R_\varepsilon = -1$, PS) presented in [11], and the Coffin-Manson (C-M) fit. The horizontal arrows indicate runout data, which are fatigue tests where no failure was observed after $4E6$ reversals; the three runouts obtained are indicated by the “x3”. As seen in the figure, the strain-life plots present very low scatter within each loading condition (i.e., $R_\varepsilon = -1$ and 0), with the exception of 0.001 mm/mm strain amplitude at $R_\varepsilon = -1$. The as-built surface roughness condition (similar for all fabricated specimens with an average $R_a = 16$ μm) could be attributed to the low scatter in the low cycle fatigue regime as it allows failure to initiate from surface micro-notches rather than sub-surface defects, which are randomly located within the part [3,11]. In the high cycle regime, materials become more sensitivity to defects [3,20], hence, the wide scatter at 0.001 mm/mm strain amplitude may be attributed to the randomly located sub-surface defects also providing an opportunity for crack initiation and propagation. Moreover, it can be seen from this figure that fatigue life (in both low and high cycle fatigue regime) is reduced for tests under $R_\varepsilon = 0$ loading due to an increase in tensile mean stress and lack of stress relaxation, which can be attributed to the relatively low ductility of the material [19]. Therefore, contrary to the fatigue behavior of wrought Ti-6Al-4V which has been found not to be sensitive to mean stress under $R_\varepsilon = 0$ loading in the low cycle fatigue regime [19], it can be concluded that as-built LB-PBF Ti-6Al-4V is sensitive to mean stress.

In order to implement the C-M model for strain-life characterization, both $R_\epsilon = -1$ data sets were used. Since the elastic strain amplitude, $\epsilon_{a,e}$, was similar to the ϵ_a , and negligible plastic strain amplitude, $\epsilon_{a,p}$, was observed, only the elastic part of the C-M model was needed and given by Eq. (1). The fatigue strength coefficient, σ'_f , and fatigue strength exponent, b , were obtained through linear regression of the $\epsilon_{a,e}$ versus $2N_f$.

$$\epsilon_a = \epsilon_{a,e} = \frac{\sigma'_f}{E} (2N_f)^b \quad (1)$$

Furthermore, as can be seen in **Fig. 3**, for the range of strain amplitudes used, the elastic portion of the C-M model accurately represents the fully reversed fatigue behavior of LB-PBF Ti-6Al-4V fabricated vertically and in the as-built/annealed condition. This is expected as LB-PBF Ti-6Al-4V is considered a relatively brittle material thus the presence of plastic deformation is minimal.

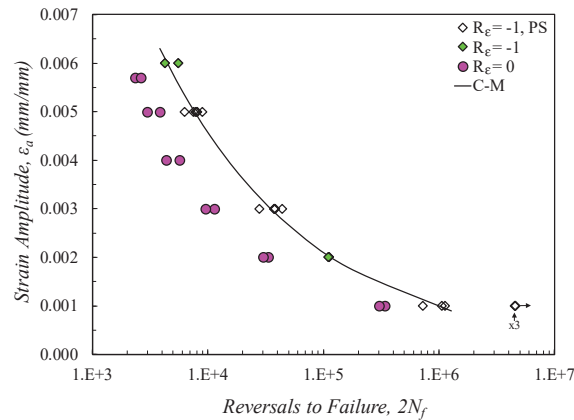


Fig. 3. Strain-life plot including fully reversed data from powder recycling study ($R_\epsilon = -1$, PS) [11], fully reversed ($R_\epsilon = -1$) and pulsating ($R_\epsilon = 0$) data from this study, and the Coffin-Manson (C-M) fit.

Since the stress-strain response of LB-PBF Ti-6Al-4V is fully elastic, the analysis of the fatigue behavior under mean stress was conducted using stress-based correction models, these include Morrow, and Smith-Watson-Topper (SWT) [20–22]. Both models are presented in Eq. (2), and (3), respectively, where σ_a is the stress amplitude, σ_{max} is the maximum stress, and σ_m is the mean stress. The purpose of the models is to provide an equivalent fully reversed stress amplitude, σ_{eq} , that yields a similar result in fatigue life as those with non-zero mean stress; then a modified version of Eq. (1) (to stress amplitude instead of strain amplitude) is used to predict fatigue life and presented in Eq. (4) [19–21,23,24]. Further details on the procedure used for the implementation of these models may be found in [19].

$$\sigma_{Morrow} = \sigma_{eq} = \frac{\sigma_a}{1 - \frac{\sigma_m}{\sigma_f}} \quad (2)$$

$$\sigma_{SWT} = \sigma_{eq} = \sqrt{\sigma_a \sigma_{max}} \quad (3)$$

$$\sigma_{eq} = \sigma_f' (2N_f)^b \quad (4)$$

The calculated fatigue lives based on the equivalent fully reversed stress amplitudes using the Morrow and SWT models versus experimental fatigue lives are presented in **Fig. 4(a)** and **(b)**, respectively. In the figures, the solid line represents a 1:1 correlation between predicted and experimental fatigue lives and the dashed lines represent scatter bands with a factor of two. Horizontal arrows indicate data points for which the predicted fatigue life was finite while the experimental life was a runout. From **Fig. 4(a)**, it can be seen that Morrow significantly underestimates the effects of mean stress, resulting in non-conservative fatigue life predictions and poor correlation ($R^2 = 0.86$) between experimental and predicted fatigue lives. On the contrary, it has been shown that Morrow is able to offer better fatigue life predictions for wrought Ti-6Al-4V [19]. The SWT model, shown in **Fig. 4(b)**, offers fatigue life predictions well within the scatter bands of two, effectively reducing scatter and providing a better correlation ($R^2 = 0.99$). Acceptable correlations obtained with the SWT approach may be explained by the ability of the model to consider that for high strength materials, with low plasticity, failure is often driven by the maximum tensile stress [12,14,20].

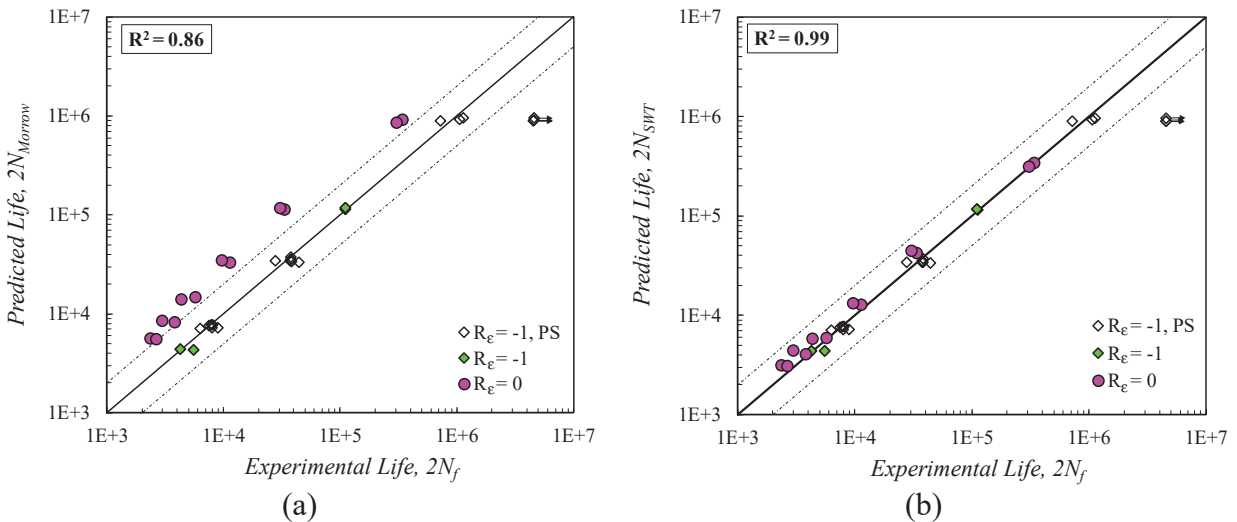


Fig. 4. Comparison of fatigue life predictions using (a) Morrow, and (b) Smith-Watson-Topper (SWT) mean stress models with experimental results.

Cumulative damage

Presented in **Fig. 5** is a semi-log plot of the strain amplitude, ϵ_a , versus cycles to failure, N_f , for $R_e = -1$ and $(R_e = -1, PS)$ [11] constant amplitude tests, as well as the second loading block

from high-low and low-high tests. The horizontal arrows indicate data runouts, the “x3” indicates runouts for $R_e = -1$, and the “x2” indicates the runouts from high-low loading. From the figure, it can be observed that the load sequence does affect the fatigue behavior of LB-PBF Ti-6Al-4V. Low-high tests that were preloaded with 0.003 mm/mm strain amplitude result in shorter fatigue lives when compared to the constant amplitude equivalents (0.006 and 0.005 mm/mm strain amplitude). The decreased fatigue life for the first load sequence may be explained by surface defects, because of the as-built surface condition, expediting crack initiation [3,20,25]. As a result, only crack propagation takes place during the second load sequence. It is important to mention that the observed behavior is not typical to conventional engineering materials [25,26]. For example, wrought Ti-6Al-4V subjected to low-high loading results in longer fatigue life for the second loading block due to material exercising during the first block [27,28]. Tests preloaded with 0.001 mm/mm strain amplitude, followed by 0.003 mm/mm strain amplitude loading (showed by the enhanced view in Fig. 5), resulted in equal or longer fatigue lives; which may be justified by the first sequence being small enough that crack initiation is not affected [20,25]. The trends observed during high-low loading may also be justified by the same surface roughness phenomena. During the high load, crack initiation and propagation are expedited due to surface defects, and during the low load, the cracks only have to propagate until failure is reached, resulting in fatigue life reduction. Finally, it was also observed that if the second sequence of high-low loading is at 0.001 mm/mm strain amplitude, the resultant stresses are not enough for crack propagation.

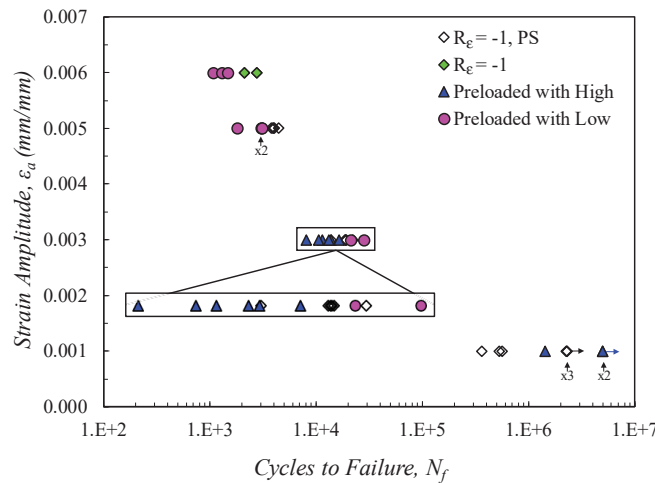


Fig. 5. Strain-life comparison of fatigue lives obtained from the second load block (i.e., low for high-low, and high for low-high) with fully reversed data generated in this study ($R_e = -1$) and a powder recycling study ($R_e = -1$, PS) [11].

The induced damage from two-level block loading, i.e., high-low and low-high, on LB-PBF Ti-6Al-4V was calculated using Miner’s rule [20,25,29] and the strain-life C-M model (see Fig. 3). Fatigue life predictions for the second loading block (i.e., remaining fatigue life) using LDR are presented versus the experimentally obtained fatigue lives in Fig. 6. In the figure, the solid line represents a 1:1 correlation between predicted and experimental fatigue lives, the dashed lines are scatter bands with a factor of two, and “x2” indicates that there are two data points. As can be seen in Fig. 6, the LDR offers rather conservative fatigue life predictions since all data

points fall below the 1:1 line. Furthermore, an $R^2 = 0.96$ indicates that the LDR is able to appropriately correlate the cumulative damage behavior of LB-PBF Ti-6Al-4V. The successful correlation of the aforementioned damage behavior using the LDR may be elucidated by the pre-existing surface defects which, regardless of loading (H-L and L-H), are able to propagate during both load sequences.

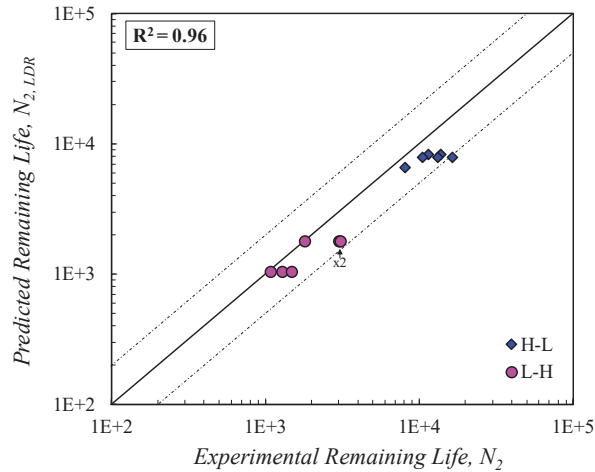


Fig. 6. Miner’s rule fatigue life predictions for the second loading block (i.e., remaining life), from high-low (H-L) and low-high (L-H) compared with experimental fatigue lives.

Conclusions

The microstructural characteristics, monotonic tensile deformation behavior, and fatigue behavior of as-built/annealed LB-PBF Ti-6Al-4V were investigated. The Morrow and Smith-Watson-Topper (SWT) mean stress correction models were employed to correlate $R_e = 0$ fatigue data. The linear damage rule (LDR) in conjunction with the Coffin-Manson (C-M) fit was used to capture the cumulative damage for high-low and low-high tests. Based on the experimental results and discussions, the following conclusions are drawn:

1. The microstructure characteristics and mechanical properties of LB-PBF Ti-6Al-4V did not present any significant differences from results found in the literature for vertically fabricated LB-PBF parts. Moreover, the monotonic stress-strain response exhibited similar values for yield and ultimate tensile stress due to negligible work hardening, which was attributed to the martensitic α' microstructure combined with the prior- β grain boundaries.
2. LB-PBF Ti-6Al-4V is sensitive to mean stress across both low and high cycle fatigue regimes.
3. The Smith-Watson-Topper mean stress correction model was able to provide appropriate fatigue life predictions while Morrow offered non-conservative predictions due to failure being driven mainly by the maximum tensile stress.
4. Relatively small load sequence effects were observed for LB-PBF Ti-6Al-4V under high-low and low-high loading. These results were justified by the as-built surface

condition enabling cracks to initiate/propagate during both blocks of the load sequences.

5. The LDR successfully correlated the cumulative damage behavior and accounted for load sequence effects for LB-PBF Ti-6Al-4V and provided conservative fatigue life predictions.

Acknowledgments

This research was partially funded by the National Science Foundation (NSF) under grant No.1657195

References

- [1] Frazier WE. Metal Additive Manufacturing: A Review. *J Mater Eng Perform* 2014;23:1917–28. doi:10.1007/s11665-014-0958-z.
- [2] Qian M, Xu W, Brandt M, Tang HP. Additive manufacturing and postprocessing of Ti-6Al-4V for superior mechanical properties. *MRS Bull* 2016;41:775–84. doi:10.1557/mrs.2016.215.
- [3] Yadollahi A, Shamsaei N. Additive manufacturing of fatigue resistant materials: Challenges and opportunities. *Int J Fatigue* 2017;98:14–31. doi:10.1016/j.ijfatigue.2017.01.001.
- [4] Lewandowski J, Seifi M. Metal Additive Manufacturing: A Review of Mechanical Properties. *Annu Rev Mater Res* 2016;46:151–86. doi:10.1146/annurev-matsci-070115-032024.
- [5] Qiu C, Adkins NJE, Attallah MM. Microstructure and tensile properties of selectively laser-melted and of HIPed laser-melted Ti-6Al-4V. *Mater Sci Eng A* 2013;578:230–9. doi:10.1016/j.msea.2013.04.099.
- [6] Simonelli M, Tse YY, Tuck C. Effect of the build orientation on the mechanical properties and fracture modes of SLM Ti-6Al-4V. *Mater Sci Eng A* 2014;616:1–11. doi:10.1016/j.msea.2014.07.086.
- [7] Bača A, Konečná R, Nicoletto G, Kunz L. Influence of Build Direction on the Fatigue Behaviour of Ti6Al4V Alloy Produced by Direct Metal Laser Sintering. *Mater Today Proc* 2016;3:921–4. doi:10.1016/j.matpr.2016.03.021.
- [8] Krakhmalev P, Fredriksson G, Yadroitsava I, Kazantseva N, Plessis A du, Yadroitsev I. Deformation Behavior and Microstructure of Ti6Al4V Manufactured by SLM. *Phys Procedia* 2016;83:778–88. doi:10.1016/j.phpro.2016.08.080.
- [9] Agius D, Kourousis KI, Wallbrink C. A Review of the As-Built SLM Ti-6Al-4V Mechanical Properties towards Achieving Fatigue Resistant Designs. *Metals* 2018;8:75. doi:10.3390/met8010075.
- [10] Murr LE, Quinones SA, Gaytan SM, Lopez MI, Rodela A, Martinez EY, et al. Microstructure and mechanical behavior of Ti-6Al-4V produced by rapid-layer manufacturing, for biomedical applications. *J Mech Behav Biomed Mater* 2009;2:20–32. doi:10.1016/j.jmbbm.2008.05.004.
- [11] Carrion PE, Soltani-Tehrani A, Phan N, Shamsaei N. Powder Recycling Effects on the Tensile and Fatigue Behavior of Additively Manufactured Ti-6Al-4V Parts. *JOM* 2019;71:963–73. doi:10.1007/s11837-018-3248-7.

- [12] Carrion PE, Imandoust A, Simsiriwong J, Shamsaei N. Effects of Layer Orientation on the Multiaxial Fatigue Behavior of Additively Manufactured Ti-6Al-4V. 29th Annu. Int. SFF Symp.- Addit. Manuf. Conf., 2018.
- [13] Kahlin M, Ansell H, Moverare JJ. Fatigue behaviour of notched additive manufactured Ti6Al4V with as-built surfaces. *Int J Fatigue* 2017;101:51–60.
- [14] Benedetti M, Fontanari V, Bandini M, Zanini F, Carmignato S. Low-and high-cycle fatigue resistance of Ti-6Al-4V ELI additively manufactured via selective laser melting: Mean stress and defect sensitivity. *Int J Fatigue* 2018;107:96–109.
- [15] Kahlin M, Ansell H, Moverare JJ. Fatigue behaviour of additive manufactured Ti6Al4V, with as-built surfaces, exposed to variable amplitude loading. *Int J Fatigue* 2017;103:353–62.
- [16] Molaei R, Fatemi A. Fatigue Design with Additive Manufactured Metals: Issues to Consider and Perspective for Future Research. *Procedia Eng* 2018;213:5–16. doi:10.1016/j.proeng.2018.02.002.
- [17] ASTM E606/E606M-12 Standard Test Method for Strain-Controlled Fatigue Testing, ASTM International, West Conshohocken, PA, 2012, https://doi.org/10.1520/E0606_E0606M-12 2012.
- [18] Bhattacharyya D, Viswanathan GB, Denkenberger R, Furrer D, Fraser HL. The role of crystallographic and geometrical relationships between α and β phases in an α/β titanium alloy. *Acta Mater* 2003;51:4679–91. doi:10.1016/S1359-6454(03)00179-4.
- [19] Carrion PE, Shamsaei N, Daniewicz SR, Moser RD. Fatigue behavior of Ti-6Al-4V ELI including mean stress effects. *Int J Fatigue* 2017;99:87–100. doi:10.1016/j.ijfatigue.2017.02.013.
- [20] Stephens RI, Fatemi A, Stephens RR, Fuchs HO. *Metal fatigue in engineering*. 2nd ed. John Wiley & Sons; 2000.
- [21] Dowling NE. Mean stress effects in strain–life fatigue. *Fatigue Fract Eng Mater Struct* 2009;32:1004–19. doi:10.1111/j.1460-2695.2009.01404.x.
- [22] Smith KN, Topper T, Watson P. A stress–strain function for the fatigue of metals (stress-strain function for metal fatigue including mean stress effect). *J Mater* 1970;5:767–78.
- [23] DOWLING NE, CALHOUN CA, ARCARI A. Mean stress effects in stress-life fatigue and the Walker equation. *Fatigue Fract Eng Mater Struct* 2009;32:163–79. doi:10.1111/j.1460-2695.2008.01322.x.
- [24] Mahtabi MJ, Shamsaei N. A modified energy-based approach for fatigue life prediction of superelastic NiTi in presence of tensile mean strain and stress. *Int J Mech Sci* 2016;117:321–33. doi:10.1016/j.ijmecsci.2016.08.012.
- [25] Fatemi A, Yang L. Cumulative fatigue damage and life prediction theories: a survey of the state of the art for homogeneous materials. *Int J Fatigue* 1998;20:9–34.
- [26] Colin J, Fatemi A, Taheri S. Fatigue Behavior of Stainless Steel 304L Including Strain Hardening, Prestraining, and Mean Stress Effects. *J Eng Mater Technol* 2010;132:021008–021008. doi:10.1115/1.4000224.
- [27] Jin O, Lee H, Mall S. Investigation into cumulative damage rules to predict fretting fatigue life of Ti-6Al-4V under two-level block loading condition. *J Eng Mater Technol* 2003;125:315–23.
- [28] Carrion PE, Shamsaei N, Moser RD. Cyclic deformation and fatigue data for Ti–6Al–4V ELI under variable amplitude loading. *Data Brief* 2017;13:180–6.
- [29] Miner MA. Cumulative Damage in Fatigue. *J Appl Mech* 1945;12:155–64.